Journal of The Electrochemical Society, 2021 **168** 110503

Monitoring SEI Formation on Graphite Electrodes in Lithium-Ion Cells by Impedance Spectroscopy

Sophie Solchenbach,[z] Xinyi Huang, Daniel Pritzl, Johannes Landesfeind, and Hubert A. Gasteiger[*]

Chair of Technical Electrochemistry, Department of Chemistry and Catalysis Research Center, Technische Universität München, Munich, Germany

In this work, we target to isolate the SEI resistance of graphite electrodes in lithium-ion cells by impedance spectroscopy measured in blocking conditions (here = 0% SOC), where the charge transfer resistance R_{CT} is significantly enlarged ($\sim 10^4$ Ω cm^2_{geom}) and thus the corresponding semicircle shifted to very low frequencies. Therefore, we measure impedance spectra of graphite/LFP full cells with a gold-wire reference electrode (GWRE) in blocking conditions (graphite potential 2 V vs Li^+/Li, 0% SOC) before and after formation. As electrolytes, we use LP57 (EC:EMC 3:7 + 1 M $LiPF_6$) either without additive or with 1 wt% VC, 1 wt% FEC, or 1 wt% DiFEC as additive. By fitting the impedance data to a transmission line-based model, we show that the SEI resistance R_{SEI} can be extracted from blocking condition impedance spectra, whereas SEI and charge transfer resistance are inseparable in non-blocking conditions. We validate our approach by determining the activation energies for the obtained ionic and SEI resistances. Finally, we introduce a potential-controlled cycling procedure which allows to assess R_{SEI} during formation. Here, we show that SEI resistance evolution follows the electrolyte reduction potentials, which makes this method a useful tool to study film formation on Li-ion battery anodes.

 [DOI: 10.1149/1945-7111/ac3158]

Manuscript submitted July 4, 2021; revised manuscript received September 28, 2021. Published November 2, 2021.

Impedance spectroscopy is a powerful in-situ analytical technique to characterize electrochemical interfaces. Thus, it has become a popular method to investigate film-forming additives in Li-ion batteries. However, to interpret impedance data is not trivial, as electronic resistances, electrolyte resistance within the separator or the electrodes, surface film resistances, diffusion processes, and the charge transfer resistances of both electrodes contribute simultaneously to the impedance spectra of a lithium-ion full cell.[1–4] 2-electrode cells with a lithium metal counter electrode ("half cells") are even less suitable for impedance measurements, as compared to porous electrodes, the impedance of lithium metal is generally larger due to its much smaller surface area, and thus dominates the half cell impedance.[5–8] Symmetric cells consisting of two identical electrodes give reliable impedance data of only cathode or anode, but require harvesting of electrodes from a cycled cell and their reassembly into symmetric cells.[9,10] To separate the contribution of cathode and anode to the full cell impedance "in-situ," a micro-reference electrode can be placed centrally between the two electrodes,[11–13] as implemented in our previous studies on Li-ion and Na-ion cells.[7,14–22]

To quantitatively evaluate impedance spectra, the data need to be fitted to a model that reflects the main physical processes of the respective electrode(s) in the measured frequency range. While electrical equivalent circuit models are often used, also analytical expressions[23,24] or numerical approaches[25] have been developed. For electrodes with commercially relevant loadings (>2 mAh cm^{-2}), the ionic resistance of the electrode pore structure contributes significantly to the total electrode impedance, resulting in a 45° feature in the high- to mid-frequency region of the impedance spectrum in a Nyquist representation.[1–3,26–29] This behavior is reflected best by transmission-line based models,[26] which account for the ionic resistance in the electrolyte phase within the pores of the electrodes, the electronic resistances of the active materials as well as interfacial impedances.[1,3,27]

The interfacial processes are commonly represented by a series of parallel resistances and capacitances (*R*/*C*) or constant phase elements (*R*/*Q*),[30] describing multiple (depressed) semicircles in a Nyquist plot. Each *R*/*C* (or *R*/*Q*) element is assigned to a physical process (contact resistance, charge transfer, surface film resistance) with a characteristic frequency f_{max}, which marks the semicircle maximum:

$$f_{max} = \frac{1}{2\pi RC} \quad [1]$$

As the contact area between electrode coating and current collector is low compared to the active surface area of the electrode, the capacitance of the corresponding *R*/*C* element is also significantly lower than that of the charge transfer or surface film resistance (the specific double-layer capacitance in battery electrolytes is typically 1–5 μF per cm^2 active surface, independent of the electrode material).[16,31] Consequently, the electrode/current collector contact resistance appears in the high-frequency region of the impedance spectrum (>10 kHz), with little interference from other electrochemical processes.[4,18] In contrast, the solid electrolyte interphase (SEI) resistance (i.e., the desolvation of Li^+-ions and their incorporation into the SEI) and the charge transfer (i.e., the intercalation of Li^+-ions from the SEI into the graphite layers) are both governed by the total surface area of the graphite active material, and the corresponding semicircles are often superimposed. As they cannot be separated, some studies evaluate both processes as one combined SEI + charge transfer *R*/*C*- or *R*/*Q*-element.[16,32,33] In other works, two *R*/*C*-type processes are fitted to the impedance spectra, and the SEI resistance on graphite is ascribed to the semicircle at higher frequencies, while the charge transfer reaction is attributed to the semicircle at lower frequencies.[8,9,30,34–37] Yet to our current understanding, it is not possible to distinguish SEI or charge transfer only based on the characteristic frequency of the two semicircles in non-blocking conditions. We see this approach especially critical if no transmission line-based model is used, as the pore resistance contribution to the impedance response might then be mistaken as part of the SEI resistance.[8,38] At even lower frequencies, diffusion in the electrolyte and solid-state diffusion in the active material appear in the impedance spectrum. While these two processes can be difficult to deconvolute, they are usually separated sufficiently in frequency from the interfacial reactions.[23,24]

However, if the lithium (de)intercalation is inhibited, the charge transfer resistance increases drastically (>1000×). At the same time, the apex of the corresponding semicircle is shifted towards much lower frequencies (see Eq. 1). The semicircles representing charge

*Electrochemical Society Fellow.
[z]E-mail: sophie.solchenbach@tum.de

transfer and SEI resistance should now be separated in frequency space. These "blocking conditions" can be reached by either using a non-intercalating electrolyte[2,28,29] or by holding the electrode at a potential where lithium (de)intercalation is not possible (i.e., at $\geqslant$2 V vs Li^+/Li in the case of graphite)[1,15,16,27,32]; the latter approach will be used in the present work. Additionally, both solid-state and electrolyte diffusion can be neglected in blocking conditions, as the absence of intercalation reaction suppresses the built-up of concentration gradients in the active material and the electrolyte.[23] Yet, to obtain meaningful results, we have to consider if and how much the SEI resistance might differ under blocking conditions compared to non-blocking conditions. First of all, previous studies show that the SEI on graphite is stable up to potentials of 2 V vs Li^+/Li, as no additional gas evolution[39] and mass change[40] was observed during cycling beyond 2 V vs Li^+/Li. Hence, we do not expect any irreversible changes to the SEI by going from non-blocking to blocking conditions at 2 V vs Li^+/Li. One could now assume that as long as the thickness and chemical composition of the SEI layer do not change with potential, the SEI resistance should be independent of potential, as was suggested by Umeda et al.[35] However, Kitz et al.[40] recently showed that while the mass of the surface film layer (as determined by EQCM-D) remains fairly constant, the resistance of a fully formed SEI on both a carbon black and a Cu model electrode changes reversibly during linear potential sweeps by about a factor of ~3. A similar dependance of the SEI resistance over SOC was found by Gordon et al.[38] This indicates a reversible potential-dependent behavior of the formed SEI resistance, which is however not caused by deposition, dissolution, or chemical changes with gaseous by-products of the SEI components. For the present study, this means that the SEI resistance measured under blocking conditions may not be quantitatively identical with the corresponding SEI resistance in non-blocking conditions. Nevertheless, SEI resistance in blocking conditions (i.e., measured at 2 V vs Li^+/Li) should still enable a semi-quantitative comparison of the SEI that is formed at different formation potentials and with different additives.

In this study, we investigate the SEI resistance in LFP/graphite cells with electrolytes either without additives or with 1 wt% vinylene carbonate (VC), 1 wt% fluoroethylene carbonate (FEC), or 1 wt% difluoroethylene carbonate (DiFEC) as additive, making use of impedance measurements in blocking conditions (i.e., at graphite potentials of ~2 V vs Li^+/Li) in combination with a gold wire micro-reference electrode (GWRE) in order to determine the impedance of the graphite electrode.[7] All of these additives are known to form an SEI layer prior to the reduction of EC.[41–43] We fit the impedance data to a transmission line-based model with two interfacial *R/Q*-elements in series, one representing the SEI resistance and the other the charge transfer resistance, as Illig et al.[3] found that this model provided the best description of the graphite electrode impedance at various states of charge (SOC) and temperatures. To further validate our approach, we determine the activation energies for ionic and SEI resistances obtained from blocking condition impedance spectra. Lastly, we subject graphite/LFP cells to a novel potential-controlled cycling procedure; by evaluating the impedance in blocking conditions after each step, we trace the SEI resistance growth during formation.

Experimental

Electrode and electrolyte preparation.—Graphite electrodes were prepared by mixing 95% graphite (T311, BET surface area 3 $m^2\ g^{-1}$, SGL Carbon, Germany) and 5% polyvinylene difluoride (PVDF, Kynar HSV 900, Arkema, France) with N-methyl pyrrolidone (NMP, anhydrous, Sigma-Aldrich, United States) in a planetary mixer (2000 rpm, 10 min). The ink (50 wt% solids content) was coated onto copper foil (MTI, United States) using a 100 μm four-edge blade and dried at 50 °C for 6 h in a convection oven, resulting in an average loading of 4.4 ± 0.3 mg cm^{-2} ($\equiv$1.6 ± 0.1 mAh cm^{-2} based on a nominal specific capacity of 360 mAh g^{-1}) with a thickness of 70 μm and a porosity of 64% (determined from the electrode thickness and from the mass loadings of graphite and PVDF, considering their bulk density of 2.3 and 1.8 g cm^{-3}, respectively). We purposely chose a low loading and high porosity to reduce the ionic resistance (which decreases with decreasing electrode thickness and increasing porosity) and to emphasize the interfacial resistance contributions (which increase with decreasing electrochemically active surface area, i.e., with decreasing loading) on the overall electrode impedance, as demonstrated by Ogihara et al.[27] Lithium iron phosphate ($LiFePO_4$, LFP) electrode sheets were purchased from Custom Cells (Itzehoe, Germany, 3.5 mAh cm^{-2}). Both coatings were punched into 11 mm electrodes.

Electrodes and separators (glass fiber, 11 mm diameter, VWR, Germany) were dried under dynamic vacuum at 120 °C for 12 h and then transferred into an argon-filled glovebox (MBraun, Germany) without exposure to air. Electrolyte solutions were prepared by adding 1 wt% vinylene carbonate (VC, BASF SE, Germany), 1 wt% fluoroethylene carbonate (FEC, BASF SE, Germany), or 1 wt% 1, 2-difluoroethylene carbonate (DiFEC, HSC Corporation, China) to a pre-mixed solution (LP57, BASF SE, Germany) of 1M $LiPF_6$ in 30 wt% ethylene carbonate (EC) and 70 wt% ethyl methyl carbonate (EMC).

Cell assembly and electrochemical testing.—Swagelok® T-cells were assembled inside an Ar-filled glovebox (MBraun, Germany) with graphite anodes and LFP cathodes, 60 μl electrolyte, 2 glassfiber separators (uncompressed: thickness 0.25 mm per separator, porosity 90%; compressed: thickness ~0.15 mm per separator, porosity ~85%; VWR, Germany), and a gold-wire reference electrode (GWRE) placed centrally between both separators.[7] Prior to cell cycling, the GWRE was lithiated by applying a charging current of 150 nA for 2 h at 45 °C (activation energy experiments) or 25 °C (all other experiments) between the LFP electrode and the GWRE. For galvanostatic formation, cells were subjected to 2 cycles at C/10 (based on a graphite specific capacity of 360 mAh g^{-1}) and 25 °C. As the lithiated GWRE has a stable potential of 0.31 V vs Li^+/Li in LFP/graphite cells (over a time of >500 h),[7] the graphite potential during formation was controlled between 1.70 V and −0.30 V vs the GWRE, corresponding to cycling the graphite potential between +2.01 and +0.01 V vs Li^+/Li. For the readers' convenience, graphite potentials that were measured vs the GWRE were converted to the Li^+/Li scale throughout this work.

Alternatively, formation was done by a novel potential-controlled cycling procedure: i) initially, the graphite potential was scanned from the OCV of the pristine graphite electrode (~3 V vs Li^+/Li) to 2.01 V vs Li^+/Li at 0.5 mV s^{-1} and held there for 30 min, after which an impedance measurement was conducted at 2.01 V vs Li^+/Li; ii) thereafter, the graphite potential was scanned from 2.01 V to 1.81 V vs Li^+/Li at 0.5 mV s^{-1} and held at this lower potential for 30 min prior to scanning the potential back to 2.01 V vs Li^+/Li at 0.5 mV s^{-1}, where the potential was held for another 30 min followed by an impedance measurement at 2.01 V vs Li^+/Li; iii) with each subsequent cycle, the lower voltage limit was first decreased from 1.81 V to 0.01 V vs Li^+/Li in steps of 0.2 V, and then raised again from 0.01 V to 1.81 V vs Li^+/Li by 0.2 V. An overview of this protocol is also shown in Fig. 5.

A single voltammetric scan was performed on pristine graphite electrodes in Swagelok® T-cells with an LFP counter and a lithium metal reference electrode (Rockwood Lithium, 450 μm, USA) at a scan rate of 0.03 mV s^{-1} between OCV (~3 V vs Li^+/Li) to 0.01 V and back to 2.0 V vs Li^+/Li.

All experiments were performed with a multi-channel potentiostat (VMP3, Biologic, France) in temperature-controlled chambers (Binder, Germany and ThermoTEC, Germany).

Electrochemical impedance spectroscopy.—Impedance spectroscopy was performed between 100 kHz and 100 mHz with a potential perturbation of 10 mV using the GWRE as a micro-

reference electrode. To improve data quality, we recorded 20 points/decade in logarithmic spacing and averaged 5 cycles per frequency. Prior to formation, impedance spectra of the pristine graphite electrodes were recorded at open circuit voltage (~3 V vs Li^+/Li) at 25 °C, which represents blocking conditions.

To achieve blocking conditions after galvanostatic formation (see above), the cells were held at 2.01 V vs Li^+/Li for 30 min, followed by an impedance measurement at 2.01 V vs Li^+/Li directly afterwards. The graphite anodes were then charged to 40% SOC at C/10. After a rest period of 30 min, the graphite impedance in non-blocking conditions (i.e., at 40% SOC) was recorded.

For activation energy experiments, impedance spectra of the pristine graphite electrodes were recorded at open circuit voltage at 5, 15, 25 35, and 45 °C. To allow for thermal equilibration, the cells were held for 30 min at each temperature prior to the impedance measurement. After galvanostatic formation (2 × C/10 at 25 °C), the cells were held at 2.01 V vs Li^+/Li and impedance was measured at 5, 15, 25 35, and 45 °C, again after 30 min hold time at each temperature to allow for thermal equilibration.

For the potential-controlled cycling procedure, an impedance measurement was performed at 2.01 V vs Li^+/Li after each potential hold step.

Data evaluation and fitting.—Micro-reference electrodes can be subject to high-frequency artefacts.[44] We tested this effect by using the reversed setup described by Raijmakers et al.[44] As the impedance magnitude of the regular and the reversed setup differs by more than 2% at frequencies above 31 kHz, only data in the frequency range between 31 kHz-100 mHz was considered for fitting of electrical equivalent circuits.[45] Fitting was performed with a MATLAB-based application ("EIS Breaker," © J. Landesfeind) based on the *fminsearch* MATLAB function using a Nelder-Mead simplex algorithm and modulus weighing. To reduce the number of free parameters, we set the exponent α of both constant phase elements Q_{SEI} and Q_{CT} to be equal, as this resulted in fits with similar residuals compared to the use of independent α-values for Q_{CT} and Q_{SEI}. The residuals versus frequency in Figs. 1–3 were calculated as the scaled difference between the measured data and fit vectors $\left(\frac{|Z(f_i)| - |Z_{fit}(f_i)|}{|Z_{fit}(f_i)|}\right)$ at the same frequency f_i (in %). Errors in tables and error bars in graphs are given as standard deviation between multiple nominally identical cells/measurements.

Results and Discussion

Graphite impedance before and after formation in blocking conditions.—As a first step towards extracting the SEI resistance from blocking conditions, we investigate how the graphite impedance in blocking conditions changes due to formation with different additives. As an example, Fig. 1a shows the Nyquist representation of a pristine graphite electrode impedance in LP57, normalized to the geometric electrode area, at OCV (~3 V vs Li^+/Li) from an LFP/graphite full cell with gold-wire reference electrode (GWRE). Fig. 1b displays a zoom-in at the high and medium frequency region of Fig. 1a. One can see a 45° transmission line at high frequencies (>150 Hz), corresponding to the ionic resistance in the electrode pores,[1,2] and an almost vertical line at frequencies below 150 Hz, which represents the double-layer capacitance between the bare graphite and the electrolyte. To extract the electrode pore resistance (R_{Pore}), we fitted the impedance spectrum of to a simplified TLM with only a constant phase element (CPE) as interfacial element (with $Z_{CPE} = ((i\omega)^{\alpha} \cdot Q_{CT})^{-1}$) and a single resistor representing the ionic resistance of the separator (R_{Sep}), as depicted in Fig. 1c.[1,2,16] The residuals of the fit are shown in Fig. 1d.

The averaged results from pristine graphite electrodes recorded in all four electrolytes (i.e., LP57 without additives or with 1 wt% of either VC, FEC, or DiFEC as additive) are shown in Table I, yielding an average pore resistance of R_{Pore} = 5.8 ± 1.0 Ω cm^2 (independent of the electrolyte, which is expected, since the additive

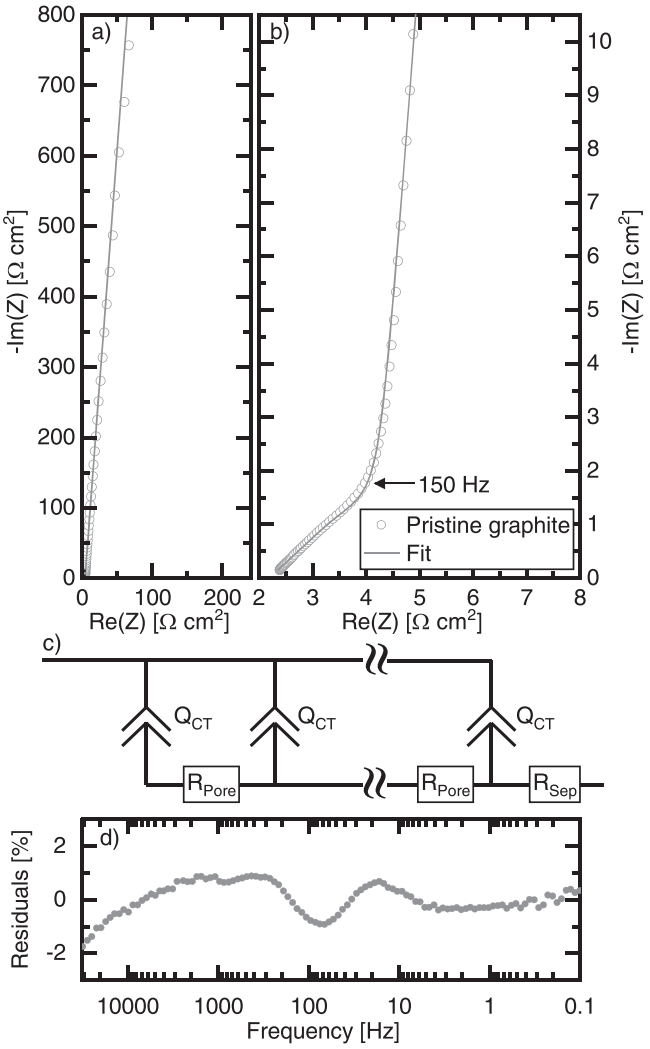

Figure 1. (a) Exemplary impedance spectrum (normalized to the geometric electrode area) of a pristine graphite electrode (gray circles) measured vs a GWRE in a graphite/LFP cell with LP57 electrolyte at OCV (~3 V vs Li^+/Li) and 25 °C. (b) Zoom-in of the high frequency region. (c) Simplified mono-rail transmission line model used to fit the data shown in (a) and (b). (d) Residuals between measured data and the fitted model.

concentrations are very low). Considering an electrode porosity of ε = 64% (uncompressed anodes), an electrode thickness of d = 70 μm, and an electrolyte conductivity of κ = 8.4 mS cm^{-1},[46] Eq. 2 yields an average electrode tortuosity τ of ~4.5 ± 0.7, which is typical for laboratory-made, highly porous graphite electrodes.[2]

$$\tau = \frac{\varepsilon \cdot R_{Pore} \cdot \kappa}{d} \quad [2]$$

The average pseudo-capacitance of 0.99 mF $s^{(\alpha-1)}$ cm^{-2}_{geom} for the pristine graphite electrodes corresponds to a specific pseudo-capacitance of 7.5 μF $s^{(\alpha-1)}$ cm^{-2}_{BET} (based on a BET surface area of 3 m^2_{BET} g^{-1} and an average of loading of 4.4 mg cm^{-2}_{geom}), which is in the same range as the previously reported 1–5 μF cm^{-2}_{BET} for battery materials in carbonate-based electrolytes.[16,31]

Next, we examine the graphite impedance spectra of the same electrodes under blocking conditions after formation. Figures 2a and 2b show the impedance of graphite electrodes at 0% SOC (i.e., at 2.01 V vs Li^+/Li) after the two formation cycles (C/10, 25 °C) in LP57 (blue squares), LP57 + 1 wt% FEC (yellow triangles), LP57 + 1 wt% VC (red diamonds), and LP57 + 1 wt% DiFEC (green triangles). All spectra approach an almost vertical line at low

Table I. Averaged parameters obtained from fitting the impedance spectra of pristine graphite electrodes (70 μm thickness, 64% porosity) in the four different electrolytes (i.e., LP57 without additives or with 1 wt% of either VC, FEC, or DiFEC as additive) to a simplified TLM (see Fig. 1c). Errors are based on standard deviations from multiple cells/measurements.

Parameter	Value
R_{Sep} [Ω cm$^2_{geom}$]	2.2 ± 0.3
R_{Pore} [Ω cm$^2_{geom}$]	5.8 ± 1.0
Q_{CT} [mF s$^{(\alpha-1)}$ cm$^{-2}_{geom}$]	0.99 ± 0.02
α [−]	0.95 ± 0.01

frequencies (see Fig. 2a), thus reaching quasi-blocking conditions. For LP57 and 1 wt% FEC electrolytes, only minor changes have occurred compared to the pristine graphite spectra: The onset of the capacitive line has shifted to slightly higher real (to ∼5.7 Ω cm^2 in Fig. 2b vs ∼4 Ω cm^2 prior to formation, as shown in Fig. 1b) and imaginary impedance values (∼3.2 Ω cm^2 vs ∼1.8 Ω cm^2). Additionally, this onset has shifted to slightly lower frequencies compared to the original ∼150 Hz of the pristine electrodes (see Fig. 1b), namely to ∼119 Hz for LP57 and to ∼106 Hz for 1 wt% FEC (see arrows in Fig. 2b). For 1 wt% VC and 1 wt% DiFEC, the difference before and after formation is more significant: The onset of the capacitive line is shifted to ∼47 and ∼23 Hz, respectively, and the real/imaginary parts of the impedance at this point have increased to ∼8.2/ ∼6.8 Ω cm^2 for 1 wt% VC and ∼12.1/∼12.7 Ω cm^2 for 1 wt% DiFEC. Summarized, all impedance spectra after formation show an impedance growth in the mid-frequency region, which we can attribute to the impedance contribution from the SEI that is formed during the two formation cycles.

To quantify the SEI resistance, the impedance spectra after formation in the different electrolytes are fitted to a suitable mono-rail TLM (see Fig. 2c). As previously proposed by Illig et al.,[3] we used two *R*/*Q* elements as interfacial elements, one for the SEI resistance (i.e., the additional resistance at medium frequencies, see Fig. 1b) and one for the charge transfer resistance (i.e., the very large resistance at low frequencies, see Fig. 1a). In general, one has to consider that also the electrode pore resistance (R_{Pore}) might increase during formation due to a decrease in electrode porosity, resulting from to the presence of a freshly formed SEI that is typically reported to have a thickness of up to 20 nm.[47,48] However, if we subtract the volume of a 20 nm thick SEI film on the graphite surface area (3 m$^2_{BET}$ g^{-1}) from the total void volume of the graphite electrode, the porosity would decrease by ∼5 percentage points (from ∼64 to ∼59%), which means that the resulting increase in the pore resistance of the graphite electrode would be <10% (see Eq. 2). Hence, the increase in ionic resistance due to SEI products is negligible for such highly porous electrodes, so that in this study the electrode pore resistance was fixed to the individual R_{Pore} of the respective pristine electrode (see Table I for the average value). The respective fits are shown by the solid lines in Figs. 2a and 2b, and the residuals are shown in Fig. 2d. The largest deviations between data and model appear at very low (<0.5 Hz) and very high (>10 kHz) frequencies, staying below 2% on average. Apparently, the additional resistance visible after formation is well represented by the added SEI *R*/*Q*-element. The summarized fitting results shown in Table II confirm that the SEI resistance after formation in LP57 + 1 wt% DiFEC is the largest (7.4 Ω cm^2), followed by LP57 + 1 wt% VC (2.5 Ω cm^2), LP57 + 1 wt% FEC (1.6 Ω cm^2), and pure LP57 (1.5 Ω cm^2). These findings agree with previous reports which showed that VC and DiFEC increase the anode impedance after formation,[7,10,14,41,42,49,50] whereas FEC shows little difference compared to a standard electrolyte without additive.[51,52]

Comparison of impedance after formation in blocking and non-blocking conditions.—Next, we would like to compare the obtained

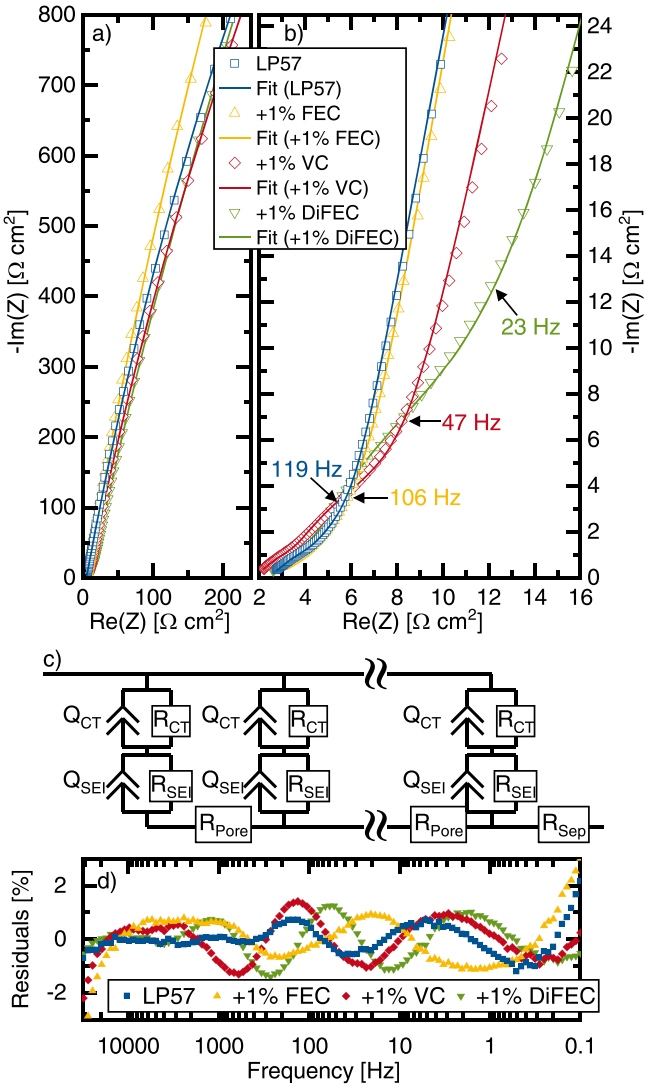

Figure 2. (a) Impedance of graphite electrodes in blocking conditions (at 0% SOC, i.e., at 2.01 V vs Li$^+$/Li) measured vs the GWRE in graphite/LFP cells at 25 °C after formation (2× C/10, 25 °C) in LP57 (1M $LiPF_6$ EC:EMC 3:7, blue squares), LP57 + 1 wt% FEC (yellow triangles), LP57 + 1 wt% VC (red diamonds), or LP57 + 1 wt% DiFEC (green triangles); the impedances are normalized to the geometric electrode area. (b) Zoom-in of the high frequency region of a). (c) Mono-rail transmission line model with two *R*/*Q*-elements used to fit the data shown in a) and b), whereby R_{Pore} was fixed to the R_{Pore} value obtained for the respective pristine graphite electrode, ranging between 5.8 ± 1.0 Ω cm^2 (see Table I). (d) Residuals between measured data and the fitted model.

SEI resistance values to the graphite impedance in non-blocking conditions. After the formation cycles, the graphite electrodes were lithiated to 40% SOC (based on the first delithiation capacity, at ∼0.12 V vs Li$^+$/Li), and the graphite impedance spectra were measured in non-blocking conditions (see Fig. 3a). All impedance spectra show a ∼45° line at high frequencies, followed by a depressed semicircle and a diffusion branch at low frequencies; the overall features of the impedance spectra represent spectra typical of graphite electrodes with areal capacities of ⩾1.5 mAh cm^{-2}.[53] Similar to the results from Fig. 2, the semicircle-like feature size depends strongly on the used additive. For LP57 electrolyte (blue squares in Fig. 3a) and LP57 + 1 wt% FEC (yellow triangles), the overall graphite impedance after formation at 40% SOC is much lower than in LP57 + 1 wt% VC (red diamonds); the highest graphite impedance is found for the LP57 + 1 wt% DiFEC electrolyte (green triangles). As these spectra in non-blocking

Table II. Averaged parameters obtained from fitting the impedance spectra of graphite electrodes after formation in LP57, LP57 + 1wt% FEC, LP57 + 1 wt% VC, and LP57 + 1 wt% DiFEC in blocking conditions (0% SOC, i.e., at 2.01 V vs Li^+/Li, see Fig. 1). The pore resistance R_{Pore} was fixed to the value obtained under blocking conditions for the respective pristine graphite electrode (for average values see Table I). Errors are based on standard deviations from multiple cells/measurements. Note that the α-value for the SEI and the charge transfer resistance were fixed to have the same value (referred to as $\alpha_{SEI,CT}$).

Parameter	LP57	+1 wt% FEC	+1 wt% VC	+1 wt% DiFEC
R_{Sep} [Ω cm^2_{geom}]	2.3 ± 0.1	2.2 ± 0.3	2.2 ± 0.5	2.2 ± 0.1
R_{SEI} [Ω cm^2_{geom}]	1.5 ± 0.2	1.6 ± 0.1	2.5 ± 0.1	7.4 ± 0.2
Q_{SEI} [mF $s^{(\alpha-1)}$ cm^{-2}_{geom}]	1.3 ± 0.2	1.1 ± 0.04	0.7 ± 0.14	0.6 ± 0.04
R_{CT} [kΩ cm^2_{geom}]	19 ± 7	16 ± 7	9 ± 2	47 ± 16
Q_{CT} [mF $s^{(\alpha-1)}$ cm^{-2}_{geom}]	0.8 ± 0.2	0.75 ± 0.04	0.97 ± 0.05	0.94 ± 0.03
$\alpha_{SEI,CT}$ [−]	0.88 ± 0.01	0.90 ± 0.01	0.86 ± 0.01	0.86 ± 0.01

conditions show only one semicircle-like feature, the TLM used to fit spectra in non-blocking conditions consisted of only one interfacial R/Q-element that represents the sum of the SEI and the charge transfer resistance, further on referred to as intercalation resistance (defined as $R_{Int} = R_{SEI} + R_{CT}$). Additionally, the equivalent circuit was extended by a constant phase element (Q_W) which accounts for the Li^+-ion diffusion in the electrolyte and the graphite electrode (see Fig. 3b). Assuming that their influence on the high- to mid-frequency region is negligible,[23] we chose this simplified representation for the diffusion processes, as they are not in the focus of the present work. The contribution of electrolyte diffusion in the separator is presumably larger than solid-state diffusion in the active material in our setup, which is why Q_W was connected in series to the TLM.[15]

Table III summarizes the fitting results, while the residuals between the measurement data and the TLM fits are shown Fig. 3c. Using only one R/Q-element in the mono-rail TLM for the impedance spectra in non-blocking conditions resulted in residuals that are mostly below 1%, except at frequencies above 10 kHz, where they reach up to 2%. This confirms the applicability of the TLM model shown in Fig. 3b for modelling the non-blocking graphite impedance data; however, this also underlines that a deconvolution of the charge transfer and the SEI resistance of the graphite electrodes cannot be achieved for non-blocking conditions under the here shown experimental conditions (i.e., no unique fit of their individual values can be obtained). Note that α_W does not correspond to 0.5, which would be expected for pure solid-state Warburg diffusion, but is around 0.6–0.68, which indicates that several processes are convoluted in the low frequency branch.[23,24]

Figures 3d and 3e compare the overall intercalation resistances (R_{Int}) from the non-blocking condition spectra at 40% SOC and the SEI resistance (R_{SEI}) from blocking condition spectra at 0% SOC after the two formation cycles. One can see that the overall trend matches well: as previously seen, DiFEC leads to a high impedance,[41] followed by VC, whereas both FEC and additive-free LP57 show a low graphite impedance. The very similar values for R_{Int} (measured at ∼0.12 V vs Li^+/Li) and R_{SEI} (measured at 2.01 V vs Li^+/Li) for a given electrolyte suggest that the SEI resistance likely represents the most significant contribution to the overall intercalation resistance of a graphite electrode in non-blocking conditions. However, a direct comparison is not possible, due to the following uncertainties: i) the quantitative potential dependence of the SEI resistance, for which a factor of ∼3 was reported by both Gordon et al.[38] (upon varying the SOC from 10%–100% SOC) and by Kitz et al.[40] (upon varying the graphite potential from 0.1–3.0 V vs Li^+/Li), while Umeda et al.[35] observed no change of R_{SEI} over ∼0%−100%SOC; ii) the different contributions of the graphite edge and basal planes in blocking and non-blocking conditions, since in blocking conditions the SEI resistance is measured over both edge and basal planes, while only the SEI at the edge planes, where lithium intercalation occurs, is visible in non-blocking conditions. Hence, it is possible that R_{SEI} in non-blocking conditions is much lower than in blocking conditions, and that R_{CT} in non-blocking conditions is not insignificant (as one could assume from the direct comparison of Figs. 3d and 3e), leading to overall similar values for R_{SEI} in blocking and R_{Int} in non-blocking conditions.

Activation energy of the SEI resistance.—While electronic and ionic resistances (i.e., R_{Pore} and R_{Sep}) only show a low temperature dependency, the effect of temperature on interfacial resistances is typically much larger.[1,3] Determining the activation energy is thus a powerful tool to classify the origin of a measured resistance.[16,18,32] To investigate the temperature behaviour of the SEI resistance, we measured the graphite impedance in blocking conditions (2.01 V vs Li^+/Li) after formation (2 × C/10 at 25 °C) in LP57, LP57 + 1 wt% FEC, LP57 + 1 wt% VC, or LP57 + 1 wt% DiFEC at 5, 15, 25, 35, and 45 °C. As before, the pore resistance (R_{Pore}) of each cell and temperature was fitted from the pristine graphite spectra under blocking conditions (see Fig. 1c); R_{Pore} for the respective temperature and graphite electrode was then fixed at this value and the blocking condition data after formation was fitted to the model shown in Fig. 2c. Figure 4 shows R_{SEI} after formation in LP57 (blue squares), LP57 + 1 wt% FEC (yellow triangles), LP57 + 1 wt% VC (red diamonds), or LP57 + 1 wt% DiFEC (green triangles) in an Arrhenius-type diagram (here represented as the 10-based logarithm of the resistance vs inverse temperature). Along with these, R_{Pore} (gray solid circles) and R_{Sep} (black open circles) from the LP57 cells without additive are shown, whereby it should be noted that the additives have no significant effect on R_{Sep} (see first row in Table II) and R_{Pore} (see Table I).

All resistances show a linear Arrhenius behavior. The apparent activation energy E_A was calculated using Eq. 3, where R_G is the universal gas constant (8.314 J mol^{-1} K^{-1}) and m is the linear regression slope of each data set in Fig. 4.

$$E_A = m \cdot R_G \cdot \ln(10) \quad [3]$$

Table IV summarizes the apparent activation energies of the different resistances. For R_{SEI}, the activation energy is around 50–70 kJ mol^{-1} and increases in the order of LP57 + 1 wt% FEC < LP57 < LP57 + 1 wt% VC < LP57 + 1 wt% DiFEC. Keefe et al.[32] recently reported an activation energy of 56–59 kJ mol^{-1} for the combined SEI + charge transfer resistance (i.e., of R_{Int}) of graphite in a similar EC-based electrolyte (1.2 M $LiPF_6$ in EC/EMC (3/7 g g^{-1})) with no additives and 58–72 kJ mol^{-1} when adding 2% VC, which is reasonably consistent with our apparent activation energy for R_{SEI} of 55 kJ mol^{-1} for LP57 without additive and 66 kJ mol^{-1} with 1 wt% VC. Similar activation energies in the range of 60–75 kJ mol^{-1} for the interfacial resistances of graphite were found even for quite different electrolyte compositions by Illig et al.[3] (in EC/EMC 1/1 with 0.1 M $LiPF_6$ plus 0.9 M $LiClO_4$) and by Schranzhofer et al.[31] (in propylene carbonate with 1 M $LiClO_4$ and 5 wt% acrylonitrile). Interestingly, Borodin et al.[54] calculated an activation energy of 64–84 kJ mol^{-1} for the ionic conductivity of lithium ethylene dicarbonate (LEDC), which is the main component of an EC-based SEI.[48] In view of the similar activation energies for

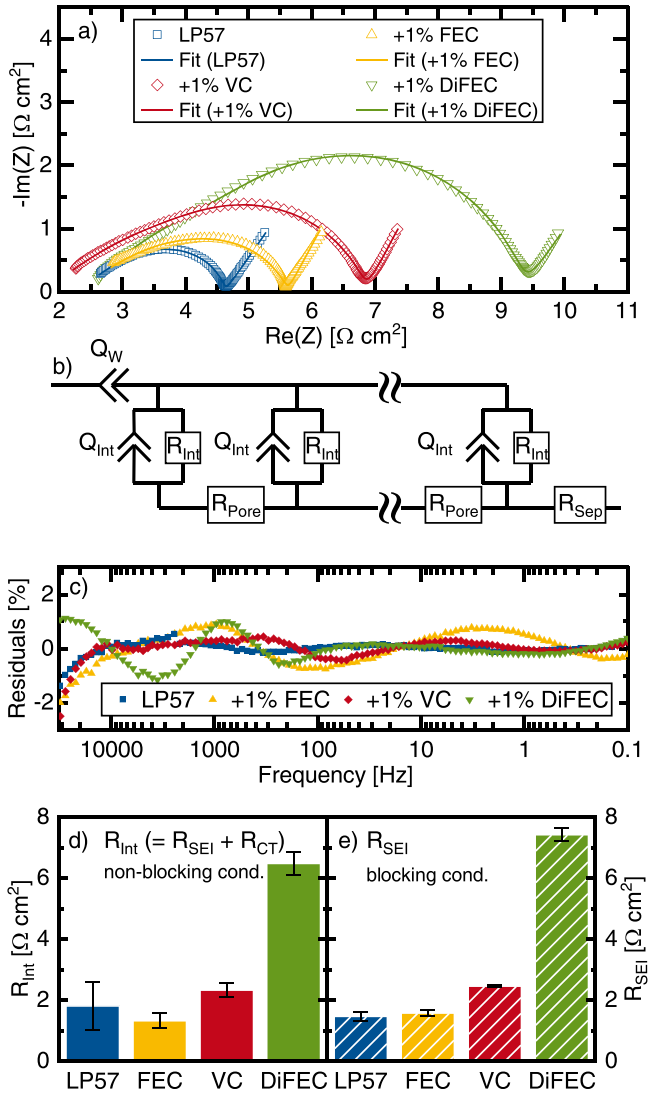

Figure 3. (a) Impedance of graphite electrodes in non-blocking conditions at 40% SOC (corresponding to ~0.12 V vs Li^+/Li) measured vs the GWRE in a graphite/LFP cell at 25 °C after formation (2× C/10, 25 °C) in LP57 (1M $LiPF_6$ EC:EMC 3:7, blue squares), LP57 + 1 wt% FEC (yellow triangles), LP57 + 1 wt% VC (red diamonds), or LP57 + 1 wt% DiFEC (green triangles); the impedances are normalized to the electrode geometric area. (b) Mono-rail transmission line model with one *R*/*Q*-element used to fit the data shown in a), whereby R_{Pore} was fixed to the R_{Pore} value obtained for the respective pristine graphite electrode, ranging between 5.8 ± 1.0 Ω cm^2 (see Table I). (c) Residuals between measured data and the fitted model. (d), (e) Comparison of the intercalation resistance R_{Int} (=R_{SEI} + R_{CT}) that was determined in non-blocking conditions at 40% SOC (data from Fig. 3(a) and R_{SEI} that was determined in blocking conditions at 0% SOC (data from Figs. 2a and 2b) for the investigated electrolytes/additives.

the ionic conductivity of LEDC and of the SEI resistance, the SEI resistance may indeed be the main contribution to the interfacial resistance of graphite under non-blocking conditions (see Figs. 3d and 3e), even though this assumption would require a quantification of R_{SEI} in non-blocking conditions that is not possible with the here used measurements.

Compared to the activation energies of the interfacial or the SEI resistance, the activation energies for R_{Sep} and R_{Pore} of ~13–15 kJ mol^{-1} are much lower, and very similar to the values found by Illig et al.[3] and Ogihara et al.[1] (14–16 kJ mol^{-1}). The very different activation energies for R_{Pore} and R_{SEI} confirm that the additional resistance evolving during formation (comp. Figures 2 and 1) is not caused by an increase in R_{Pore} (as was already argued above based on the estimated negligible effect of the SEI on the electrode void volume), but by the interfacial barrier imposed by the SEI. A systematic understanding of the activation energy of the SEI formed with different additives might be helpful to improve the low- and high temperature performance of graphite electrodes. For example, the lower activation energy of an SEI formed in FEC compared to LP57 without additive or with VC additive might contribute to its success as a low-temperature additive.[55]

Monitoring SEI formation with impedance measurements in blocking conditions.—Depending on the electrolyte and additives used, the SEI forms on graphite between 1.5–0.5 V vs Li^+/Li.[43,48,56,57] Unfortunately, the charge transfer resistance changes drastically within this potential range,[16] which makes it difficult to directly observe SEI formation by impedance spectroscopy. However, we can use impedance measurements in blocking conditions to make the SEI formation visible. Therefore, we developed a potential-controlled cycling procedure, which is shown in Fig. 5. In this procedure, after an initial impedance measurement of the pristine graphite electrode at OCV (~3 V vs Li^+/Li), the potential of the electrode is scanned at 0.5 mV s^{-1} from OCV to 2.01 V vs Li^+/Li, where the potential is held for 30 min, followed by a potential-controlled impedance measurement (the times at which impedance measurements are conducted are indicated by the orange stars in Fig. 5). Subsequently, the potential is scanned to successively lower potentials (in increments of 0.2 V), at which it is held again for 30 min prior to scanning back into blocking conditions (i.e., to 2.01 V vs Li^+/Li) in order to again conduct an impedance measurement after a further potential hold of 30 min at 2.01 V vs Li^+/Li. At such a high potential, the electrolyte reduction reactions are not taking place (as will also be seen later in Fig. 6a), so that to a first approximation the SEI is maintained in the state that was formed in the preceding lower potential (e.g., impedance measurement marked by the third orange star in Fig. 5 would represent the properties of the SEI that was formed at 1.81 V vs Li^+/Li). By repeating this procedure from lower potentials of 1.81 to 0.01 V (solid gray arrow) and back to 1.81 V vs Li^+/Li (dashed gray arrow), we can follow the SEI evolution by evaluating the corresponding impedance spectra taken under blocking conditions at 2.01 V vs Li^+/Li. The corresponding SEI resistance (R_{SEI}) is obtained from fitting the equivalent circuit shown in Fig. 3c, whereby R_{Pore} is again fixed to the value obtained for the respective pristine electrode at the initial OCV.

To first determine the onset of electrolyte reduction for the four electrolyte solutions, we also performed slow voltage scans (0.03 mV s^{-1}) from OCV to 0.01 V vs Li^+/Li on pristine graphite electrodes in graphite/LFP cells with a lithium metal reference electrode (see Fig. 6a). As stated above, no electrolyte reduction currents are observed at the potential of 2.01 V vs Li^+/Li, where the impedance spectra under blocking conditions are acquired. The observed potential peaks for electrolyte reduction (see dotted vertical lines in Fig. 6a) increase in the order LP57 (blue line) < LP57 + 1 wt% VC (red line) < LP57 + 1 wt% FEC (yellow line) < LP57 + 1 wt% DiFEC (green line), in agreement with previous studies.[41,42,56,57]

Figures 6b–6d show the R_{SEI} values obtained by fitting the impedance spectra under blocking conditions (i.e., at 2.01 V vs Li^+/Li) spectra in this potential-controlled cycling procedure (see Fig. 5), using the same approach that was applied for the data analysis shown in Fig. 2. The R_{SEI} values are plotted vs the lower potential applied in the same step. The arrows in Figs. 6b–6d indicate the direction of stepping: First the lower potential is stepwise decreased from 1.81 to 0.01 V vs Li^+/Li (solid gray arrow), and then increased from 0.01 V to 1.81 V vs Li^+/Li (dashed gray arrow). In LP57 electrolyte without additives (see Fig. 6b), R_{SEI} increases to ~1.5 Ω cm^2 between 0.8–0.4 V vs Li^+/Li and remains constant thereafter, which matches with the LP57 reduction peak at ~0.7 V vs Li^+/Li in Fig. 6a. The VC-containing electrolyte shows a slow rise of R_{SEI} between 1.4–0.8 V to ~0.8 Ω cm^2 and a stronger

Table III. Averaged parameters obtained from fitting the impedance spectra of graphite electrodes after formation in LP57, LP57 + 1wt% FEC, LP57 + 1 wt% VC, and LP57 + 1 wt% DiFEC in non-blocking conditions at 40% SOC (corresponding to ~0.12 V vs Li^+/Li, see Fig. 3a) to the mono-rail transmission line model shown in Fig. 3b. In both cases, the pore resistance R_{Pore} was fixed to the value obtained under blocking conditions for the respective pristine graphite electrode (for average values see Table I). Errors are based on standard deviations from multiple cells/measurements.

Parameter	LP57	+1 wt% FEC	+1 wt% VC	+1 wt% DiFEC
R_{Sep} [Ω cm^2_{geom}]	2.1 ± 0.2	2.1 ± 0.2	2.2 ± 0.5	2.2 ± 0.1
R_{Int} [Ω cm^2_{geom}]	1.8 ± 0.8	1.3 ± 0.2	2.3 ± 0.2	6.5 ± 0.4
Q_{Int} [mF $s^{(\alpha-1)}$ cm^{-2}_{geom}]	0.83 ± 0.06	0.81 ± 0.3	0.9 ± 0.1	0.82 ± 0.14
α_{Int} [−]	0.84 ± 0.01	0.85 ± 0.08	0.79 ± 0.02	0.82 ± 0.05
Q_W [F $s^{(\alpha-1)}$ cm^{-2}_{geom}]	1.1 ± 0.1	1.1 ± 0.1	0.9 ± 0.2	1.3 ± 0.1
α_W [−]	0.60 ± 0.02	0.64 ± 0.05	0.67 ± 0.02	0.68 ± 0.05

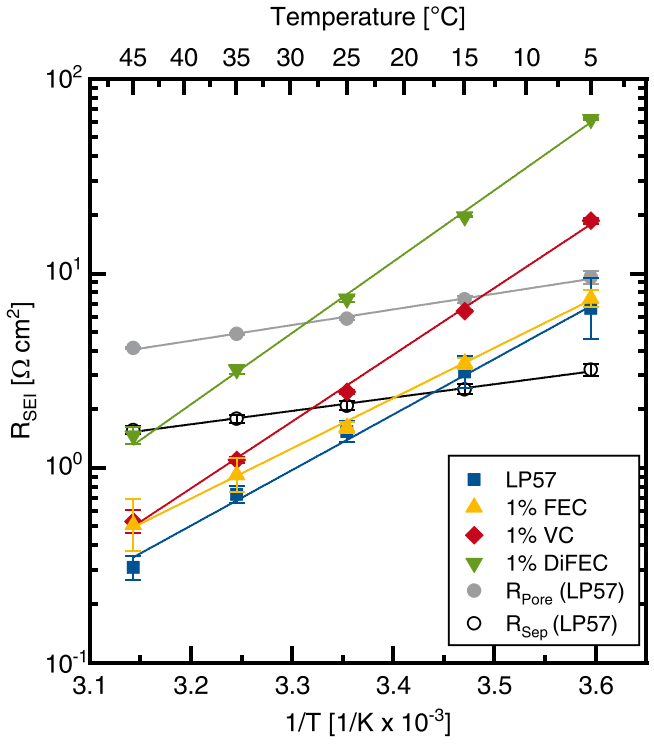

Figure 4. Arrhenius representation of R_{SEI} obtained from impedance spectra fits of graphite electrodes in blocking conditions (at 2.01 V vs Li^+/Li) at 5, 15, 25, 35 and 45 °C after formation (2 × C/10, 25 °C) in LP57 (blue squares), LP57 + 1 wt% FEC (yellow triangles), LP57 + 1 wt% VC (red diamonds), and LP57 + 1 wt% DiFEC (green triangles); the model shown in Fig. 2c was used for the fits. For comparison, R_{Pore} (gray solid circles) and R_{Sep} (black open circles) obtained from fitting the impedance spectra of the pristine graphite electrodes in LP57 to the model shown in Fig. 1c are also given. Errors are based on standard deviations from multiple cells/measurements.

growth between 0.8–0.4 V to ~2 Ω cm^2 (Fig. 6c). The reductive current of the VC-containing electrolyte (red line in Fig. 6a) reflects this development, as between 1.7 and 0.9 V vs Li^+/Li, the reduction current increases linearly, until it peaks at ~0.8 V vs Li^+/Li. During the positive-going steps (from right to left in Fig. 6c), R_{SEI} grows slightly from ~2 to ~2.2 Ω cm^2, suggesting that the evolution of the SEI, i.e., the radical-catalyzed polymerization of VC, continues.[14,43,56–60] With FEC (Fig. 6d), R_{SEI} increases rapidly to ~1.4 Ω cm^2 between 1.4–1.0 V vs Li^+/Li and remains constant thereafter; accordingly, the reduction current for LP57 + 1 wt% FEC recedes after a peak at 1.2 V (see yellow line in Fig. 6a). For these three electrolytes, i.e., for LP57 without additive, LP57 + 1 wt% FEC, and LP57 + 1 wt% FEC, the R_{SEI} values after one complete cycle of the potential-controlled cycling procedure are essentially identical with the values obtained after the two galvanostatic formation cycles (see Table II), confirming that comparable SEIs are formed by our here proposed potential-controlled cycling procedure to monitor the formation of the SEI.

The SEI resistance in the DiFEC electrolyte (Fig. 6e) appears already at ~1.6 V and rises to 1 Ω cm^2 until ~1.0 V, concurrent with a large reduction peak between 1.9–1.2 V (green line in Fig. 6a). Apparently, this initial SEI is not sufficiently passivating, as we see a significant reduction current between 1.0–0.6 V along with a continuous rise of R_{SEI} to 2.8 Ω cm^2 between 1.0–0.2 V vs Li^+/Li. The SEI impedance grows further to 3.5 Ω cm^2 during the positive-going steps, which is however still lower than the R_{SEI} of 7.4 Ω cm^2 after two galvanostatic formation cycles (see Table II). This difference suggests a strong dependence of the SEI formation with DiFEC on the exact formation procedure, different to what was observed for the other three electrolytes.

To investigate whether SEI formation is completed after one cycle of the potential-controlled cycling procedure shown in Fig. 5, we subjected the cells to a second potential-controlled cycle and recorded the graphite impedance in blocking conditions thereafter. The fitted values of R_{SEI} values after the first and the second cycle in blocking conditions are shown in Fig. 7. Interestingly, the SEI resistance for both electrolytes with either 1 wt% VC or 1 wt% FEC stays constant, whereas R_{SEI} grows to ~1.8 Ω cm^2 for LP57 (still being very close to the ~1.5 Ω cm^2 obtained after two galvanostatic formation cycles, see Table II) and to ~3.8 Ω cm^2_{geom} for the electrolyte with DiFEC, which is still lower than the ~7.4 Ω cm^2 obtained after two galvanostatic formation cycles (see Table II).

Summarizing the findings from Figs. 6 and 7, the evolution of the SEI resistances combined with the electrolyte reduction potentials give valuable insights into the SEI formation dynamics in the different electrolytes. As expected, the SEI formation in LP57 occurs simultaneously with the reduction of EC, yet the slight increase in resistance during the second cycle points towards a further SEI growth (which is however still within the error bar of R_{SEI} in the first cycle). The FEC-containing electrolyte forms an SEI at substantially higher potentials compared to LP57; this SEI not only has a very low resistance and remains constant over time, but also exhibits the lowest activation energy (see Table IV), which is advantageous for low-temperature operation. This self-limiting growth behaviour of FEC is likely the reason why FEC can be used in high concentrations as an electrolyte co-solvent,[61] which is not the case for other additives. While the SEI formed by VC is also stable over time (at least after the first cycle), it has a higher resistance and is assumed to grow by a radical polymerization reaction;[14,43,56–60] accordingly, the amount of VC has to be carefully adjusted to not create a highly resistive SEI.[7,14,50] The SEI formed in the electrolyte with DiFEC starts to evolve at the most positive potential of all tested additives, but grows continuously, resulting in a highly resistive SEI after only few cycles. Additionally, the SEI resistance with DiFEC grows even throughout the second cycle, which indicates that the passivating properties of DiFEC on graphite are inferior to VC or FEC.

Table IV. Activation energies of R_{SEI} after two formation cycles of graphite electrodes in LP57, LP57 + 1 wt% FEC, LP57 + 1 wt% VC, or LP57 + 1 wt% DiFEC determined under blocking conditions at 2.01 V vs Li^+/Li. In addition, the activation energies for R_{Sep} and R_{Pore} of pristine graphite electrodes in LP57 are listed. All values were determined from the linear regression slopes in Fig. 4. Errors are based on standard deviations from multiple cells/measurements.

Electrolyte	Activation energy [kJ mol^{-1}]
R_{SEI} in LP57	54.7 ± 1.9
+ 1% FEC	49.4 ± 0.9
+ 1% VC	65.8 ± 1.4
+ 1% DiFEC	70.2 ± 1.9
R_{Sep} (LP57)	13.2 ± 0.5
R_{Pore} (LP57)	15.4 ± 0.5

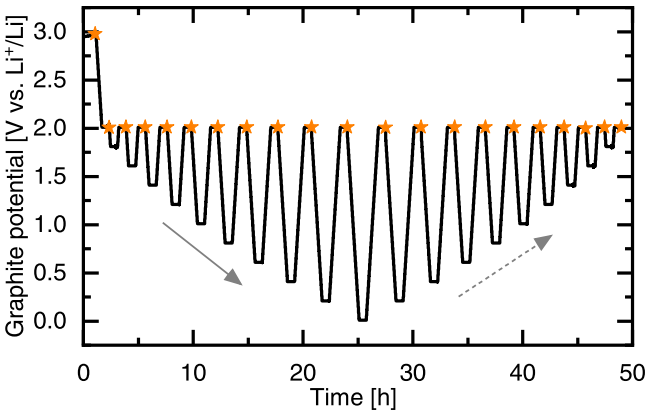

Figure 5. Graphite potential during the potential-controlled cycling procedure conducted at 25 °C. The graphite potential was controlled vs the GWRE (0.31 V vs Li^+/Li) and is reported here versus Li^+/Li. Each step consists of a voltage scan at 0.5 mV s^{-1} to a lower potential, where the potential is held for 30 min; thereafter, the potential is scanned back at 0.5 mV s^{-1} to 2.01 V vs Li^+/Li (i.e., into blocking conditions), where after a 30 min potential hold an impedance measurement is performed (marked by the orange stars). With each step, the lower potential is first decreased by 0.2 V increments down to 0.01 V vs Li^+/Li (solid gray arrow) and then raised by 0.2 V between 0.01–1.81 V vs Li^+/Li (dashed gray arrow).

Conclusions

In this work, we analyse the SEI resistance (R_{SEI}) of graphite electrodes from impedance spectra in blocking conditions, i.e., at a potential of 2.01 V vs Li^+/Li, where the charge transfer resistance of graphite electrodes is significantly enlarged ($\sim 10^4$ Ω cm^2), resulting in a shift of the associated impedance feature to very low frequencies. We demonstrated that the SEI resistance can be isolated from impedance spectra in blocking conditions using a transmission line model (TLM) fit with a predetermined pore resistance (R_{Pore}), whereby the latter is obtained from the impedance analysis of the pristine graphite electrodes at the initial OCV prior to formation. On the other hand, in non-blocking conditions (here at 40% SOC), the SEI and the charge transfer resistance (R_{CT}) are indistinguishable, and only their sum can be determined from the impedance spectra. With this method, we investigated the SEI resistance of graphite electrodes in an LP57 electrolyte (EC/EMC (3/7 g/g) with 1 M $LiPF_6$) without additives as well as in LP57 containing 1 wt% VC, 1 wt% FEC, or 1 wt% DiFEC. By determining the activation energies of the pore and the SEI resistances, we could exclude the effect of a changed electrode porosity and thus confirm the used model. Amongst these four electrolytes, LP57 + 1 wt% FEC results in the most stable SEI that has a very low R_{SEI} with the lowest activation energy, which explains why it can be used at high

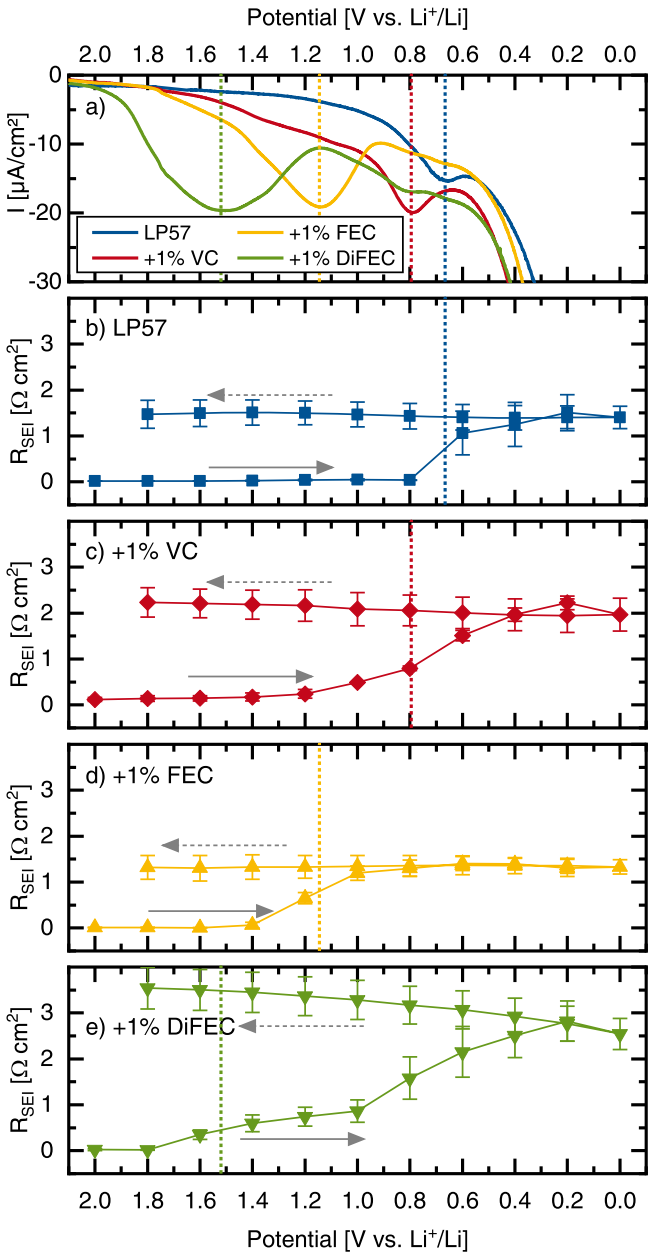

Figure 6. (a) Current density vs potential during reductive voltammetric scans (0.03 mV s^{-1}) of pristine graphite electrodes in a graphite/LFP T-cell with lithium metal reference electrode with LP57 (blue line), LP57 + 1 wt% VC (red line), LP57 + 1 wt% FEC (yellow line), or LP57 + 1 wt% DiFEC (green line) electrolyte. (b)–(e) R_{SEI} after each potential step (see procedure in Fig. 5) in graphite/LFP cells with a GWRE, obtained from fitting impedance spectra in blocking conditions to the model shown in Fig. 2c. The dotted vertical lines mark the maximum of the respective reduction peak in a). The gray arrows indicate the direction of R_{SEI} evolution. Errors are based on standard deviations from multiple cells/measurements.

concentrations (i.e., as co-solvent) and why it is favourable at low temperatures.

Finally, we used a potential-controlled cycling procedure that allowed us to determine R_{SEI} at different stages during formation. Here, we showed that the SEI resistance appears at the respective electrolyte reduction potentials. Additionally, we found that SEI formation in LP57 without additives as well as with 1 %wt VC or FEC additives is largely completed after the electrolyte reduction peak in the first cycle, whereas the SEI in the electrolyte with DiFEC continues to grow both after electrolyte reduction during the first cycle as well as throughout further cycling. Hence, this novel

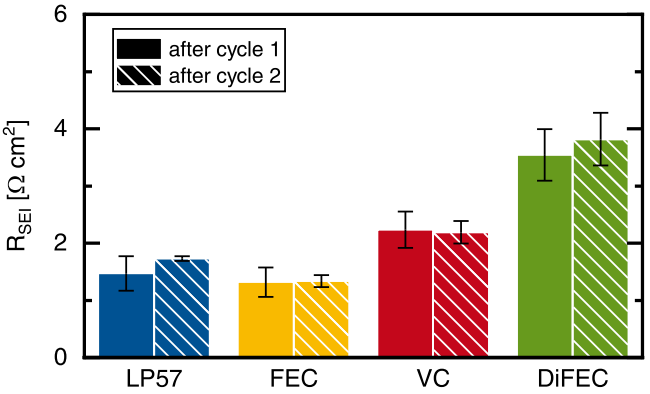

Figure 7. SEI resistance (R_{SEI}) after the first complete cycle (solid bars) and the second complete cycle (dashed bars) of the potential-controlled cycling procedure (see Fig. 5), obtained from fitting impedance spectra of graphite electrodes cycled in LP57 (blue bars), LP57 + 1 wt% FEC (yellow bars), LP57 + 1 wt% VC (red bars), and LP57 + 1 wt% DiFEC (green bars) in blocking conditions (i.e., at 2.01 V vs Li^+/Li) to the equivalent circuit shown in Fig. 2c. Errors are based on standard deviations from multiple cells/measurements.

method is a helpful tool to study SEI film formation kinetics on Li-ion battery electrodes, for example during different formation procedures or cycling at different temperatures.

Acknowledgments

Financial support by the BASF SE through its Research Network on Electrochemistry and Batteries is gratefully acknowledged. J. L. gratefully acknowledges the funding by the BMBF (Federal ministry of Education and research, Germany) for its financial support under the auspices of the ExZellTUM II project, grant number 03XP0081. The authors would like to thank Prof. Bharatkumar Suthar and Robert Morasch for very fruitful discussions.

ORCID

Sophie Solchenbach https://orcid.org/0000-0001-6517-8094
Daniel Pritzl https://orcid.org/0000-0002-9029-107X
Johannes Landesfeind https://orcid.org/0000-0003-0333-2185
Hubert A. Gasteiger https://orcid.org/0000-0001-8199-8703

References

1. N. Ogihara, S. Kawauchi, C. Okuda, Y. Itou, Y. Takeuchi, and Y. Ukyo, *J. Electrochem. Soc.*, **159**, A1034 (2012).
2. J. Landesfeind, J. Hattendorff, A. Ehrl, W. A. Wall, and H. A. Gasteiger, *J. Electrochem. Soc.*, **163**, A1373 (2016).
3. J. Illig, M. Ender, A. Weber, and E. Ivers-Tiffée, *J. Power Sources*, **282**, 335 (2015).
4. M. Gaberscek, J. Moskon, B. Erjavec, R. Dominko, and J. Jamnik, *Electrochem. Solid-State Lett.*, **11**, A170 (2008).
5. J. Y. Song, H. H. Lee, Y. Y. Wang, and C. C. Wan, *J. Power Sources*, **111**, 255 (2002).
6. R. Hernandez-Maya, O. Rosas, J. Saunders, and H. Castaneda, *J. Electrochem. Soc.*, **162**, A687 (2015).
7. S. Solchenbach, D. Pritzl, E. J. Y. Kong, J. Landesfeind, and H. A. Gasteiger, *J. Electrochem. Soc.*, **163**, 2265 (2016).
8. M. Steinhauer, S. Risse, N. Wagner, and K. A. Friedrich, *Electrochim. Acta*, **228**, 652 (2017).
9. C. H. Chen, J. Liu, and K. Amine, *J. Power Sources*, **96**, 321 (2001).
10. R. Petibon, C. P. Aiken, N. N. Sinha, J. C. Burns, H. Ye, C. M. VanElzen, G. Jain, S. Trussler, and J. R. Dahn, *J. Electrochem. Soc.*, **160**, A117 (2013).
11. J. Zhou and P. H. L. Notten, *J. Electrochem. Soc.*, **151**, A2173 (2004).
12. D. P. Abraham, S. D. Poppen, A. N. Jansen, J. Liu, and D. W. Dees, *Electrochim. Acta*, **49**, 4763 (2004).
13. M. Ender, A. Weber, and E. Ivers-Tiffée, *J. Electrochem. Soc.*, **159**, A128 (2012).
14. D. Pritzl, S. Solchenbach, M. Wetjen, and H. A. Gasteiger, *J. Electrochem. Soc.*, **164**, A2625 (2017).
15. J. Landesfeind, D. Pritzl, and H. A. Gasteiger, *J. Electrochem. Soc.*, **164**, A1773 (2017).
16. D. Pritzl, J. Landesfeind, S. Solchenbach, and H. A. Gasteiger, *J. Electrochem. Soc.*, **165**, A2145 (2018).
17. M. Wetjen, S. Solchenbach, H. A. Gasteiger, D. Pritzl, J. Hou, and V. Tileli, *J. Electrochem. Soc.*, **165**, 1503 (2018).
18. D. Pritzl, A. E. Bumberger, M. Wetjen, J. Landesfeind, S. Solchenbach, and H. A. Gasteiger, *J. Electrochem. Soc.*, **166**, A582 (2019).
19. F. Linsenmann, D. Pritzl, and H. A. Gasteiger, *J. Electrochem. Soc.*, **166**, A3668 (2019).
20. T. Teufl, D. Pritzl, M. A. Mendez, S. Solchenbach, and H. A. Gasteiger, *J. Electrochem. Soc.*, **166**, A1275 (2019).
21. F. Linsenmann, D. Pritzl, and H. A. Gasteiger, *J. Electrochem. Soc.*, **168**, 010506 (2021).
22. R. Morasch, B. Suthar, and H. A. Gasteiger, *J. Electrochem. Soc.*, **167**, 100540 (2020).
23. J. Huang and J. Zhang, *J. Electrochem. Soc.*, **163**, A1983 (2016).
24. G. Sikha and R. E. White, *J. Electrochem. Soc.*, **154**, A43 (2007).
25. A. Shodiev, E. N. Primo, M. Chouchane, T. Lombardo, A. C. Ngandjong, A. Rucci, and A. A. Franco, *J. Power Sources*, **454**, 227871 (2020).
26. R. de Levie, *Electrochim. Acta*, **8**, 751 (1963).
27. N. Ogihara, Y. Itou, T. Sasaki, and Y. Takeuchi, *J. Phys. Chem. C*, **119**, 4612 (2015).
28. R. Morasch, J. Landesfeind, H. A. Gasteiger, and B. Suthar, *J. Electrochem. Soc.*, **165**, A3459 (2018).
29. J. Landesfeind, M. Ebner, A. Eldiven, V. Wood, and H. A. Gasteiger, *J. Electrochem. Soc.*, **165**, A469 (2018).
30. M. D. Levi and D. Aurbach, *J. Phys. Chem. B*, **5647**, 4630 (1997).
31. H. Schranzhofer, J. Bugajski, H. J. Santner, C. Korepp, K.-C. Möller, J. O. Besenhard, M. Winter, and W. Sitte, *J. Power Sources*, **153**, 391 (2006).
32. A. S. Keefe, S. Buteau, I. G. Hill, and J. R. Dahn, *J. Electrochem. Soc.*, **166**, A3272 (2019).
33. T. S. Ong and H. Yang, *J. Electrochem. Soc.*, **149**, A1 (2002).
34. D. Aurbach, M. D. Levi, E. Levi, H. Teller, B. Markovsky, and G. Salitra, *J. Electrochem. Soc.*, **145**, 3024 (1998).
35. M. Umeda, K. Dokko, Y. Fujita, M. Mohamedi, I. Uchida, and J. R. Selman, *Electrochim. Acta*, **47**, 885 (2001).
36. B. K. Antonopoulos, F. Maglia, F. Schmidt-Stein, J. P. Schmidt, and H. E. Hoster, *Batter. Supercaps*, **1**, 110 (2018).
37. O. S. Mendoza-Hernandez, H. Ishikawa, Y. Nishikawa, Y. Maruyama, Y. Sone, and M. Umeda, *Electrochim. Acta*, **131**, 168 (2014).
38. I. J. Gordon, S. Grugeon, H. Takenouti, B. Tribollet, M. Armand, C. Davoisne, A. Débart, and S. Laruelle, *Electrochim. Acta*, **223**, 63 (2017).
39. S. Solchenbach, G. Hong, A. T. S. Freiberg, R. Jung, and H. A. Gasteiger, *J. Electrochem. Soc.*, **165**, A3304 (2018).
40. P. Kitz, M. Lacey, P. Novák, and E. J. Berg, *Anal. Chem.*, **91**, 2296 (2019).
41. L. Ma, S. L. Glazier, R. Petibon, J. Xia, J. M. Peters, Q. Liu, J. P. Allen, R. N. C. Doig, and J. R. Dahn, *J. Electrochem. Soc.*, **164**, 5008 (2017).
42. J. Xia, R. Petibon, A. Xiao, W. M. Lamanna, and J. R. Dahn, *J. Electrochem. Soc.*, **163**, A1637 (2016).
43. K. U. Schwenke, S. Solchenbach, J. Demeaux, B. L. Lucht, and H. A. Gasteiger, *J. Electrochem. Soc.*, **166**, A2013 (2019).
44. L. H. J. Raijmakers, M. J. G. Lammers, and P. H. L. Notten, *Electrochim. Acta*, **259**, 517 (2018).
45. S. Solchenbach, (2018), PhD Thesis, Technische Universität München.
46. Y. Qian, C. Schultz, P. Niehoff, T. Schwieters, S. Nowak, F. M. Schappacher, and M. Winter, *J. Power Sources*, **332**, 60 (2016).
47. F. Jeschull, J. Maibach, K. Edström, and D. Brandell, *J. Electrochem. Soc.*, **164**, 1765 (2017).
48. M. Nie, D. Chalasani, D. P. Abraham, Y. Chen, A. Bose, and B. L. Lucht, *J. Phys. Chem. C*, **117**, 1257 (2013).
49. R. Petibon, E. C. Henry, J. C. Burns, N. N. Sinha, and J. R. Dahn, *J. Electrochem. Soc.*, **161**, A66 (2013).
50. J. C. Burns, R. Petibon, K. J. Nelson, N. N. Sinha, A. Kassam, B. M. Way, and J. R. Dahn, *J. Electrochem. Soc.*, **160**, A1668 (2013).
51. I. A. Profatilova, S.-S. Kim, and N.-S. Choi, *Electrochim. Acta*, **54**, 4445 (2009).
52. M. Klett, J. A. Gibson, S. E. Trask, B. J. Polzin, A. N. Jansen, D. W. Dees, and D. P. Abraham, *J. Electrochem. Soc.*, **163**, A875 (2016).
53. R. Morasch, J. Keilhofer, H. A. Gasteiger, and B. Suthar, *J. Electrochem. Soc.*, **168**, 080519 (2021).
54. O. Borodin, G. V. Zhuang, P. N. Ross, and K. Xu, *J. Phys. Chem. C*, **117**, 7433 (2013).
55. B. Liu, B. Li, and S. Guan, *Electrochem. Solid-State Lett.*, **15**, A77 (2012).
56. B. Zhang, M. Metzger, S. Solchenbach, M. Payne, S. Meini, H. A. Gasteiger, A. Garsuch, and B. L. Lucht, *J. Phys. Chem. C*, **119**, 11337 (2015).
57. B. Strehle, S. Solchenbach, M. Metzger, K. U. Schwenke, and H. A. Gasteiger, *J. Electrochem. Soc.*, **164**, A2513 (2017).
58. H. Ota, Y. Sakata, A. Inoue, and S. Yamaguchi, *J. Electrochem. Soc.*, **151**, A1659 (2004).
59. M. Nie, J. Demeaux, B. T. Young, D. R. Heskett, Y. Chen, A. Bose, J. C. Woicik, and B. L. Lucht, *J. Electrochem. Soc.*, **162**, A7008 (2015).
60. L. El Ouatani, R. Dedryvère, C. Siret, P. Biensan, and D. Gonbeau, *J. Electrochem. Soc.*, **156**, A468 (2009).
61. T. Teufl, B. Strehle, M. Philipp, H. A. Gasteiger, and M. A. Mendez, *J. Electrochem. Soc.*, **165**, 2718 (2018).